Society of Petroleum Engineers

SPE-184983-MS

Water-Soluble Solvent as an Additive to Steam for Improved SAGD

Kai Sheng, Ryosuke Okuno, and Mingyuan Wang, The University of Texas at Austin

This paper was prepared for presentation at the SPE Canada Heavy Oil Technical Conference held in Calgary, Alberta, Canada, 15-16 February 2017.

Abstract

Coinjection of solvent with steam results in lower chamber-edge temperatures than those in steam-assisted gravity drainage (SAGD), which enable to decrease heat losses to the overlying formation rocks. However, use of highly volatile solvents, such as propane, can yield significantly slow bitumen production due to low chamber-edge temperatures. The objective of this research is to investigate the potential of water-soluble solvent as an additive to steam for reducing steam-oil ratio (SOR) while keeping SAGD-like rates of bitumen production.

The chamber-edge temperature for a given overall composition and operating pressure is defined as the temperature at which the vapor phase completely condenses with decreasing temperature. Thermodynamic predictions show that the chamber-edge temperature so defined will increase substantially if the solvent can partition into the aqueous phase at chamber-edge conditions. This is confirmedin numerical reservoir simulation for coinjection of steam with dimethyl ether (DME), as a water-soluble solvent, for Athabasca bitumen. In simulation case studies, coinjection of steam with DME (DME-SAGD) is compared with SAGD and coinjection of steam with C_4 (C_4-SAGD), in terms of SOR, bitumen production, local displacement efficiency, and solvent recovery. The steam-injection pressure is 35 bars for all cases, and 2 mol% of solvent is coinjected in solvent-SAGD simulations until the steam chamber reaches the side boundary of a 2-D homogeneous reservoir model.

DME is more volatile and less soluble in bitumen than C_4 at their corresponding chamber-edge conditions. However, results show that DME-SAGD results in 35% lower SOR than SAGD while being able to increase bitumen-production rates of SAGD. Analysis of simulation results indicates that the solubility of DME in water not only makes the chamber-edge temperature higher than that of C_4-SAGD, but also yields15% higher solvent-recovery factor than C_4-SAGD. The main reason for the latter observation is that a much smaller fraction of the injected solvent is present in the vapor phase in DME-SAGD than in C_4-SAGD. Also, DME dissolves in both water and bitumen, which results in the aqueous and oleic phases of nearly-equal density within the gravity-drainage zone near the edge of a steam chamber. This is the neutral regime of oil-water two-phase flow along the chamber edge between the two extreme cases: SAGD and C_4-SAGD. Unlike in C_4-SAGD, the reduced gravity segregation in DME-SAGD is expected to facilitate the mixing of condensed solvent with bitumen near the edge of a steam chamber.

1. Introduction

In-situ recovery of heavy oil and bitumen is challenging because they are highly viscous, and usually are immobile at reservoir conditions (Butler 1997). Steam-assisted gravity drainage (SAGD) is the most widely-used method of bitumen recovery. In SAGD, steam is injected into the bitumen reservoir through an (upper) horizontal well and forms a steam-saturated zone, which is called a "steam chamber." At the edge of a steam chamber, the vapor (V) phase completely condenses, and releases its latent heat. The heated oil and steam condensate drain by gravity to the (lower) horizontal well that is located 4 – 8 m below and parallel to the injection well. Although only a part of the heat can be added to the oleic (L) phase in the reservoir, it effectively increases the L-phase mobility since viscosity of bitumen is highly sensitive to temperature. The main drawback of SAGD is the significant usage of energy and water to generate steam, which also results in a large amount of green-house-gas emission.

A widely-used parameter to quantify the energy efficiency of steam injection processes is the cumulative steam-to-oil ratio (CSOR), defined as the ratio of the cumulative volume of steam injected (cold water equivalent) to the cumulative volume of bitumen produced. CSOR is particularly sensitive to heat losses to the overlying formation rocks. In SAGD, elevated temperatures (e.g., 450 – 520 K) occur within the steam chamber and in regions beyond the chamber edge located in its vicinity. Shen (2013) stated that, for SAGD to be economically feasible, the energy efficiency measured by CSOR is generally in the range of 2 – 4 m^3/m^3. It is desirable to operate at low chamber temperatures while maintaining economically sustainable rates of oil production so that the CSOR can be reduced. SAGD is expected to be even less energy-efficient for highly heterogeneous reservoirs (Venkatramani and Okuno 2017). Thus, there is a critical need to reduce SAGD's CSOR from both environmental and economic standpoints, which has motivated the search for alternative processes.

Coinjection of steam and solvent for SAGD (solvent-steam-assisted gravity drainage, or solvent-SAGD) has been studied and pilot-tested as a potential method to improve the drawbacks of SAGD (Leaute 2002; Gupta et al. 2005; Leaute and Carey 2007; Gupta and Gittins 2006). Solvent-SAGD processes proposed in the literature, such as expanding-solvent-SAGD (ES-SAGD), solvent-aided-process (SAP) and liquid-addition-to-steam-for-enhanced-recovery (LASER), use a small amount of solvents (e.g., a few to 20 percent by liquid volume equivalent) (Leaute 2002; Gupta et al. 2005; Leaute and Carey 2007; Gupta and Gittins 2006). They attempt to enhance the L-phase mobility by the dilution of oil by solvent, in addition to the thermal energy released from the injected steam, to reduce the steam requirement. It is reported in the literature that solvent-SAGD, if properly designed, can increasebitumen-drainage rate and displacement efficiency, while reducing CSOR (e.g., EnCana's SAP pilot and Imperial Oil's LASER) (Nasr et al. 2003; Gates 2007; Gupta et al. 2005; Gupta and Gittins 2006; Leaute 2002; Leaute and Carey 2007; Li et al. 2011ab; Keshavarz et al. 2014 and 2015).

Prior investigations into solvent-SAGD are mainly concerned with hydrocarbon solvents, such as propane, butane, and diluents, which usually consist of pentane and heavier hydrocarbons at different concentrations (Nasr et al. 2003; Gates 2007; Ivory et al. 2008; Li et al. 2011a and 2011b; Keshavarz et al. 2014 and 2015). The hydrocarbon solvents that are reported to be suitable have vapor pressures that are close to that of water at an operating pressure: e.g., n-hexane and n-heptane as single-component solvents for various bitumen reservoirs (Li et al. 2011a; Mohebati et al. 2012; Keshavarz et al. 2015). However, such hydrocarbon solvents are relatively expensive, and in-situ retention of the coinjected solvent, which inevitably happens under heterogeneity, can substantially affect the project's economics.

In general, more volatile solvents are less expensive. Therefore, they are of lower risk for injection into bitumen/heavy-oil reservoirs. Also, it is expected that mixing of bitumen with more volatile solvent results in lower viscosity of the resulting oil mixture at a given mixing ratio, temperature, and pressure. As will be explained in the next section, however, coinjection of steam with highly volatile solvents (e.g., propane and butane) substantially lowers the temperature at the edge of a steam chamber (in comparison with

steam-only injection), which lowers the L-phase mobility. For example, prior investigations have shown that coinjection of propane with steam is unlikely advantageous over SAGD at the operating conditions in most target reservoirs, especially for Athabasca bitumen reservoirs (Li et al. 2011b; Keshavarz et al. 2015). Results presented in the literature show that lowering the temperature at the edge of a steam chamber by coinjection of volatile solvents with steam reduces heat losses to the overlying formation rocks, but the operating chamber-edge temperature should not be too low to maintain a SAGD-like oil production rate (Keshavarz et al. 2014 and 2015; Venkatramani and Okuno 2016). A practical way to improve the efficiency of SAGD is to develop effective strategies for solvent-SAGD that result in less consumption of energy and water while keeping a SAGD-like rate of bitumen production.

This paper is motivated by the question as to how we can use the water component and/or the aqueous (W) phase to improve the efficiency of steam-based oil recovery, such as SAGD and cyclic steam stimulation. This is because water is by far the most dominant component in steam-based oil recovery for heavy-oil and bitumen recovery (Zhu and Okuno 2016). The volume of produced water is a few times greater than the volume of produced oil in SAGD and cyclic steam stimulation. The central hypothesis in this research is that the combined mechanisms for enhancement of bitumen mobility by heat and dilution are more effective with water-soluble solvents than the conventional alkane-based solvents.

As will be presented in this paper for the first time, thermodynamic calculations and flow simulations on the basis of experimental data indicate that the solubility of solvent in water is expected to effectively utilize the thermal and compositional mechanisms for enhancing bitumen mobility in the reservoir. In this research, dimethyl ether (DME) is considered as a water-soluble solvent, although it is not the purpose of this paper to single out DME as a promising additive to steam to improve SAGD.

DME is the lightest organic in the ether family with the chemical formula of CH_3-O-CH_3. DME can be synthesized in a variety of ways at low costs, for example, from methanol, organic waste, and biomass. The second lightest ether is diethyl ether, but it is highly reactive. Therefore, DME is the only ether considered in this research.

DME is a colorless gas with mild sweet odor at standard conditions. It liquefies under moderate pressure or cooling (Ratnakar et al. 2016a). DME is betweenpropane (C_3) and n-butane (C_4) in terms of volatility, and soluble in oil as presented in the experimental studies (Ihmels et al. 2007; Wu et al. 2008). Other properties of DME, such as density, viscosity and critical parameters, are reported in the literature (Wu et al. 2003; Wu et al. 2004; Ihmels et al. 2007). Due to its slight polarity, DME is also soluble in water (Ratnakar et al. 2016a, b). However, there area limited amount of experimental data for DME/water and DME/oil mixtures. Experimental studies of DME/water binary phase behavior were presentedby Pozo and Streett (1984) and Holldorff and Knapp (1988). Park et al. (2007) conducted an experimental study for phase behavior of DME/decane and DME/dodecane mixtures. Chernetsky et al. (2015) measured densities and viscosities of DME/oil mixtures. Ratnakar et al. (2016a, b) presented phase-behavior data of DME/oil/brine. However, phase behavior of DME/bitumen/brine mixtures has not been presented in the literature.

Recently, novel applications of DME in petroleum reservoir engineering werepresented in the literature. Coreflooding studies and field studies indicated that DME can be an effective solvent for enhanced water-flooding processes (Chernetsky et al. 2015; Parsons et al. 2016; Chahardowli et al. 2016; Groot et al. 2016a; Groot et al. 2016b; Alkindi et al. 2016; te Riele et al. 2016). The DME injected can be efficiently recovered through the produced water due to the solubility in water, and the produced water that contains DME can be re-used (Chernetsky et al. 2015; Parsons et al. 2016). Furthermore, Ganjdanesh et al. (2016) presented that DME can be used to treat condensate and water blocks in hydraulic-fractured shale-gas condensate reservoirs through numerical investigation by taking advantage of DME distribution in the W and L phases and its high volatility.

Thermodynamic modeling for the application of DME to petroleum engineering processes has been studied. Cubic equations of state (EOSs), such as Robinson and Peng (PR)(1978), with the van der Waals

(vdW) mixing rulesare not entirely satisfactoryformodeling DME/water mixtures (Ratnakar et al. 2016a, b). Accurate modeling of hydrogen-bonding and polar interactions usually requires more advanced EOSs and/or mixing rules, such as cubic-plus-association (CPA) EOS and the Huron-Vidal (HV) mixing rule (Huron and Vidal 1979; Chapman et al. 1986; Michelsen 1990; Kontogeorgis et al. 1996; Folas et al. 2006a and 2006b; Oliveira et al. 2007; Pedersen et al. 2014; Ratnakar et al. 2016a, b). Ratnakar et al. (2016a) used the CPA EOS based on Soave-Redlich-Kwong (Soave 1972) to calculate partitioning of DMEin the W and L phases for DME/oil/brine mixtures. Ratnakar et al. (2016b) used the PR EOS with the HV mixing rule to model phase behavior of DME/brine/oil mixtures.

The primary objective of this paper is to present, for the first time, potential benefits of using water-soluble solvents as steam additives to improve the efficiency of SAGD, along with the mechanisms involved. To study the effect of solvent's solubility in water on oil recovery in solvent-SAGD, the secondary objective is to compare DME-steam coinjection (DME-SAGD) with coinjection of steam with volatile alkanes, such as C_4, of which the volatility is close to DME. The research is based on thermodynamic calculations and flow simulations; however, experimental data available for relevant fluids are used to calibrate the numerical models. The significance of the paper lies in the mechanistic explanation of how water-soluble solvents are expected to make differences in temperature and component distributions during SAGD and its variants. Optimal conditions for DME-SAGD are beyond the scope of the current paper because DME has been taken merely as an example of water-soluble solvent.

The next section presents thermodynamic calculations for chamber-edge conditions for SAGD and solvent-SAGD with different solvents, such as DME and alkanes. This will explain the impact of solvent's solubility in water on chamber-edge conditions. Then, a simulation case study will compare SAGD and solvent-SAGD with DME and C_4 in terms of bitumen-production rate, CSOR, ultimate bitumen recovery, and solvent recovery.

2. Vapor-condensation conditions for water/solvent/bitumen

Oil drainage by gravity occurs mainly along the edge of a steam chamber in SAGD and its variants (Keshavarz et al. 2014). Therefore, the temperature-composition conditions near the steam-chamber edge substantially affect the efficiency of solvent-SAGD in terms of oil production and energy/water consumption at a given operating pressure (Keshavarz et al. 2014 and 2015; Venkatramani and Okuno 2016). In general, there are three phases inside a steam chamber: the vapor (V), aqueous (W), and oleic (L) phases. At the edge of a steam chamber, the V phase completely condenses, making hot water (water condensate) from the vapor water and liquid solvent from the vapor solvent. This liquid solvent is then mixed with heated, mobile bitumen through mechanical dispersion along and outside the edge of a steam chamber (Venkatramani and Okuno 2017). In solvent-SAGD, therefore, the L-phase mobility becomes higher not only by the thermal mechanism, but also bythe compositional mechanism.

The thermodynamic conditions at the edge of a steam chamber in solvent-SAGD depend substantially on the phase behavior of water/solvent/bitumen mixtures (Keshavarz et al. 2014 and 2015; Venkatramani and Okuno 2016). More specifically, such conditions are determined by vapor condensation, in which a phase transition occurs between two phases (WL) and three phases (WLV), in the water/solvent/bitumen system at a given operating pressure and overall composition. Figure 1 schematically illustrates the chamber-edge (or vapor-condensation) conditions in a ternary diagram for water/pentane/bitumen at a chamber-edge temperature at the operating pressure of 35 bars. The red dot in the ternary diagram (Figure 1a) indicates an overall composition on the boundary between WL and WLV, which corresponds to a point on the edge of a steam chamber (Figure 1b) at the specified pressure.

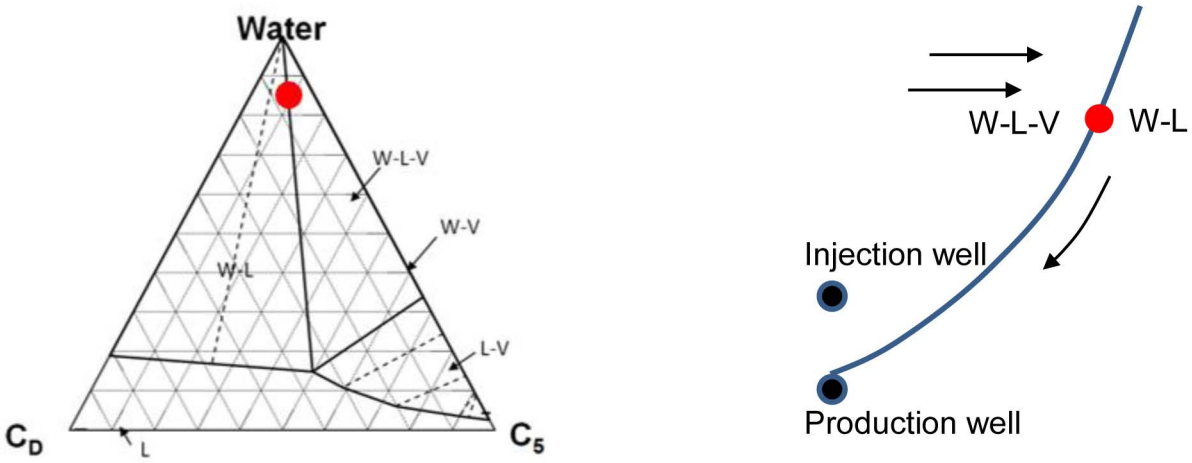

a. Ternary diagram b. Schematic of chamber edge

Figure 1—Thermodynamic conditions at the edge of a steam chamber corresponding to vapor-condensation conditions. The ternary diagram shows an overall composition on the edge of a tie triangle of W, L, and V at 35 bars for the water/pentane/bitumen system as an example. "C_D" stands for the dead-oil pseudo component, which is bitumen in this example. The chamber schematic shows a point on the edge of a steam chamber, of which the thermodynamic conditions correspond to the red dot in the ternary diagram.

This section provides an analysis of chamber-edge (i.e., vapor-condensation) conditions for SAGD and solvent-SAGDat a given pressure, 35 bars as an example. The solvents used for solvent-SAGD are DME and alkanes, ranging from C_3 to n-hexane (C_6). Ternary mixtures consisting of water, bitumen, and solvent are used in this section. First, the phase-behavior models usedare described in sections 2.1 and 2.2. Then, the impact of water-soluble solvent (taking DME as an example) on vapor-condensation conditions are analyzed in section 2.3.

2.1 EOS models for water/n-alkane/bitumen

The PR EOS (Robinson and Peng 1978) with the vdW mixing rules isused for phase-equilibrium calculation of water/n-alkane/bitumen mixtures. Tables 1 and 2 summarize parameters for the PR-EOS models with the vdW mixing rules, such as critical properties and binary interaction parameters (BIPs). Critical properties of water and n-alkanes are based on the American Petroleum Institute (API) technical data book (1983) and group contribution methods (Constantinou and Gani 1994; Constantinou et al. 1995) as summarized in Venkatramani and Okuno (2015). The dead-bitumen component ("C_D" in Tables 1 and 2) is the Athabasca bitumen characterized by Kumar and Okuno (2016) ("Bitumen A" in their paper).

Table 1—Critical properties and molecular weight (MW) for components.

Components	T_C, K	P_C, bar	ω	MW, g/mol	V_C, cc/mol
C_1	190.56	45.99	0.0157	16.04	–
C_3	369.83	42.48	0.1543	44.10	203
n-C_4	425.12	37.96	0.2014	58.12	255
n-C_5	469.70	33.70	0.2511	72.15	304
n-C_6	507.60	30.25	0.3010	86.18	370
C_D	847.17	10.64	1.0406	530.00	1330
Water	647.10	220.64	0.3433	18.01	–
DME	400.05	52.92	0.2000	46.07	–

Table 2—Binary interaction parameters (BIPs) for the PR EOS with the vdW mixing rules. All other BIPs are zero. C_D stands for the dead-bitumen component.

BIP	C_1	C_3	n-C_4	n-C_5	n-C_6	C_D
C_D	0.000	0.067	0.075	0.081	0.088	0.000
Water	0.732	0.666	0.636	0.607	0.579	0.169
DME	0.000	0.000	0.000	0.000	0.000	0.015

A BIP correlation for water with alkanes was developed for reliable estimation of water solubility in alkanes on the basis of the PR EOS (Venkatramani and Okuno 2015), as follows:

$$\mathrm{BIP}_{w/HC} = c_1[1 + \exp(c_2 - c_3 MW)]^{-1/c_4}, \quad (1)$$

where $c_1 = 0.24200$, $c_2 = 65.90912$, $c_3 = 0.18959$, and $c_4 = -56.81257$. MW is the molecular weight of n-alkane. This correlationis based on experimental data for water/alkane three-phase behavior (Brunner 1990). The solubility of alkanes in water has beenmeasured to bevery low; e.g., up to 0.1 mol% as reported by Scharlin et al. (1998). The PR EOS with the BIP correlation given in Equation 1 usually underestimates the solubility of alkanes in water (Venkatramani and Okuno 2015); that is, alkanes are essentially insoluble in water, and partitiononly into the vapor and oleic phases in this research. For the BIP of water withC_D, the value from Equation 1 is multiplied by 0.7 to account for the effect of aromaticityof the bitumen (C_D) on the solubility of water in bitumen. The scaling factor of 0.7 was obtained by Venkatramani and Okuno (2016) by matching experimental data for Athabasca bitumen measured by Amani et al. (2013a and b). BIPs between bitumen and n-alkanes are calculated by the following correlation (Kumar 2016):

$$\mathrm{BIP}_{bit/sol} = 0.0349 \ln\left(\frac{V_{C-sol}}{V_{C-bit}}\right) + 0.1329, \quad (2)$$

where V_C is critical volume. $V_{C\text{-}sol}$ is the standard value for the alkane solvent of interest. $V_{C\text{-}bit}$ can be calculated directly from Riazi and Daubert's correlation (1987).

2.2 EOS model for water/DME/bitumen

The vdW mixing rules are inaccurate for modeling water/DME mixtures, especially for three-phase conditions and solubility of DME in water. For example, if the PR EOS with the vdW mixing rules is calibrated with three-phase conditions for water/DME mixtures (Pozo and Streett 1984), the average absolute relative deviation (AARD)forthe DME solubility in water is more than 45% on the basis of Pozo and Streett (1984). Therefore, the PR EOS with the Huron-Vidal (HV) mixing rule (Huron and Vidal 1979) is used for modeling water/DME/bitumen mixtures, as in Ratnakar et al. (2016b), in which they used the HV mixing rule for calibrating a DME/brine/oil system with experimental data and predicting the partitioning of DME into the L and W phases.

Properties of water and $C_D$are the same as in the water/n-alkane/bitumen models. Vapor-pressure datafor DME, such as critical temperature (T_C), critical pressure (P_C), and acentric factor (ω), were taken from Tallon and Fenton (2006), as shown in Table 1. However, experimental data for mixtures of DME with other components are scarce. As explained below, therefore, interaction parameters for DME/C_D (Table 2) and water/DME were calibrated with experimental data.

For DME/hydrocarbon mixtures, the only data that are relevant to this research and available in the literature are given by Park et al. (2007) for the DME solubility in n-decane (C_{10}) and n-dodecane (C_{12}). A BIP of 0.015 has been found to give an AARD of 1.5% for these data. Although the BIP of DME with bitumen is expected to be different, 0.015 is also used for the DME/$C_D$pair in the absence of any other relevant data (Table 2).

The HV parameters forthe water/DMEpair were obtained by matchingthe data for three-phase conditions and DME solubility in waterup to 493 K and 509 bars (Pozo and Streett 1984). The randomness parameters for components j and k are 0.131 for the two ways (jk and kj), where j is water and k is DME. The energy parameters for j (water) and k (DME) are $g_{jk} = g_{jk}' + g_{jk}'' T$, where g_{jk}' is −1000 and g_{jk}'' is −0.570, and $g_{kj} = g_{kj}' + g_{kj}' T$, where g_{kj}' is 1370 and g_{kj}' is 1.290. Unlike the vdW mixing rules, the HV mixing ruleexhibitsimproved accuracy for DME solubility in water and three-phase conditions. AARDs for three-phase temperature and DME solubility in water with the HV mixing rule are 0.9% and 17.3%, respectively. The corresponding average absolute deviation (AAD)is 3.8 K for three-phase temperature and 2.1 mol% for DME solubility in wateron the three-phase curve. Figure 2 also comparesEOS predictionswith experimental data of Pozo and Streett (1984). In this figure, the horizontal line for each temperature represents the three-phase pressure for the W, V, and L phases. Above the three-phase pressure, two different two-phase regions (W-L and L-W) are present (not shown in Figure 2). Below it, the W-V region is present.

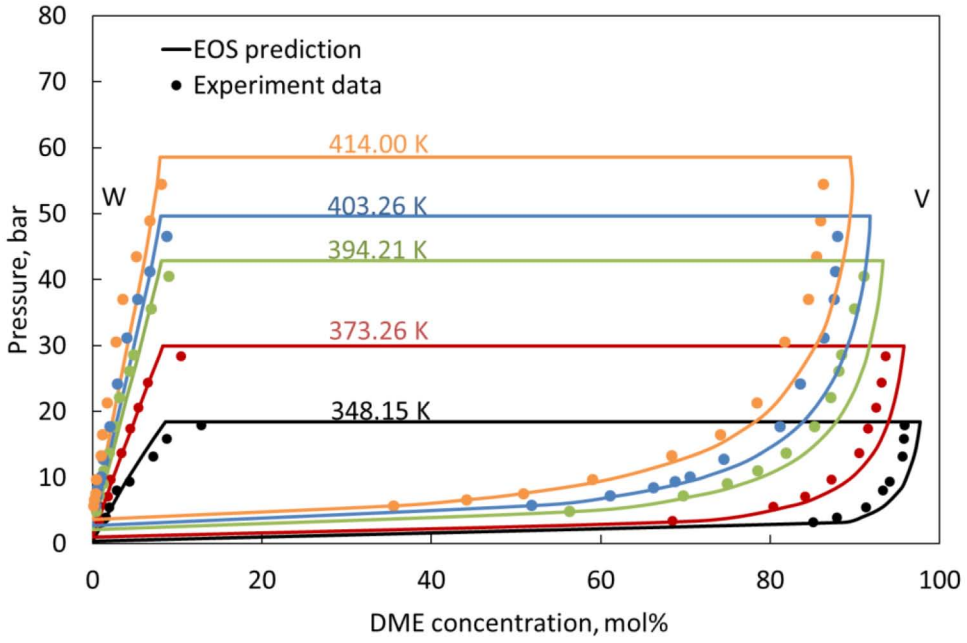

Figure 2—Pressure-composition (P-x) diagrams for water/DME mixtures at 5 different temperatures. The data were taken from Pozo and Streett (1984). The predictions are based on the PR EOS with the HV mixing rule. The horizontal line for each temperature represents the three-phase conditions for the W, V, and L phases.

2.3 Analysis of vapor-condensation temperature at 35 bars

This subsection presents the difference between alkanes and DME in terms of phase behavior when they are mixed with water and bitumen at a given pressure, 35 bars, on the basis of the EOS models (see sections 2.1 and 2.2). Differences come from the solubility in water that is much greater for DME than for alkanes (Figure 2). The main objective in this section is to explain the potential impact of this difference on vapor-condensation (or chamber-edge) temperature for water/solvent/bitumen mixtures in solvent-SAGD.

Figure 3 shows vapor-pressure curves of solvent components and three-phase curves for water/solvent binaries based on the EOS models described in sections 2.1 and 2.2. Vapor-pressure curves in this figure show that DME is between C_3 and C_4 in terms of volatility. However, the interaction of DME with water is apparently different from that of n-alkanes with water. For example, the three-phase curve forthe water/DME binary is on the higher-temperature side of DME's vapor-pressure curve (Pozo and Streett 1984). However, the three-phase curve fora water/n-alkane binary is observed to be the lower-temperature side of vapor pressure curve for that n-alkane (Brunner 1990).

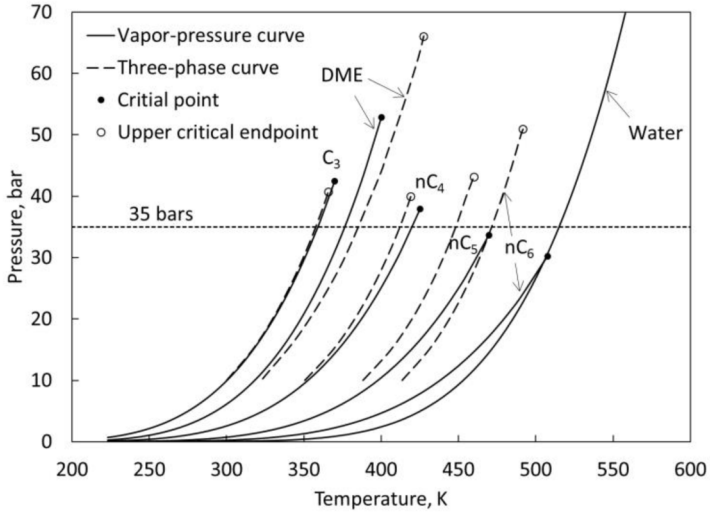

Figure 3—Vapor pressure curves of pure components and three-phase curves for water/solvent binaries. UCEP stands for upper critical endpoint, at which three-phase behavior culminates.

Figure 4 compares different alkane solvents in terms of vapor-condensation temperature for a typical overall composition (95 mol% water, 4 mol% solvent, and 1 mol% bitumen) for a solvent-SAGD chamber edge at 35 bars. In this figure, two-phase regions associated with the tie triangle are omitted for clarity. The vapor-condensation temperature is calculated to be 358 K for propane, 415 K for butane, 453 K for pentane, and 476 K for hexane. That is, it monotonically increases with decreasing volatility of the alkane solvent used. The vapor-condensation temperature for the propane case is remarkably lower than that for the hexane case ($\Delta T = 118$ K), which substantially reduces the mobility of the resulting L phase. This largely explains the result of previous studies that n-hexane is more suitable than propane as an additive to steam for solvent-SAGD for Athabasca bitumen (Keshavarz et al. 2015; Li et al. 2011a; Mohebati et al. 2012).

As mentioned before, the volatility of DME is between those of propane and butane. Therefore, one may expect the vapor-condensation temperature can be as low as the propane and butane cases, as shown in Figure 4. Figure 5 shows the ternary diagram calculated for the water/DME/bitumen system at the same conditions used for Figure 4. The vapor-condensation temperature for the DME case is calculated to be 442 K (Figure 5), which is higher than the propane and butane cases and even close to the pentane case (Figure 4). Since the overall composition near the edge of a steam chamber is always in the vicinity of 100% water in SAGD and its variants, the phase-transition temperature from WLV to WL is sensitive to the solubility of solvent in water (or the composition of the W phase that is equilibrium with L and V) at a given operating pressure. The hypothesis obtained from these calculations is that vapor-condensation temperature at a given pressure and composition will increase substantially if the solvent can partition into the W phase at operating conditions. This will beconfirmed in numerical reservoir simulations for coinjection of steam with different solvents, such as DME and C_4, for Athabasca bitumen at 35 bars in the next section.

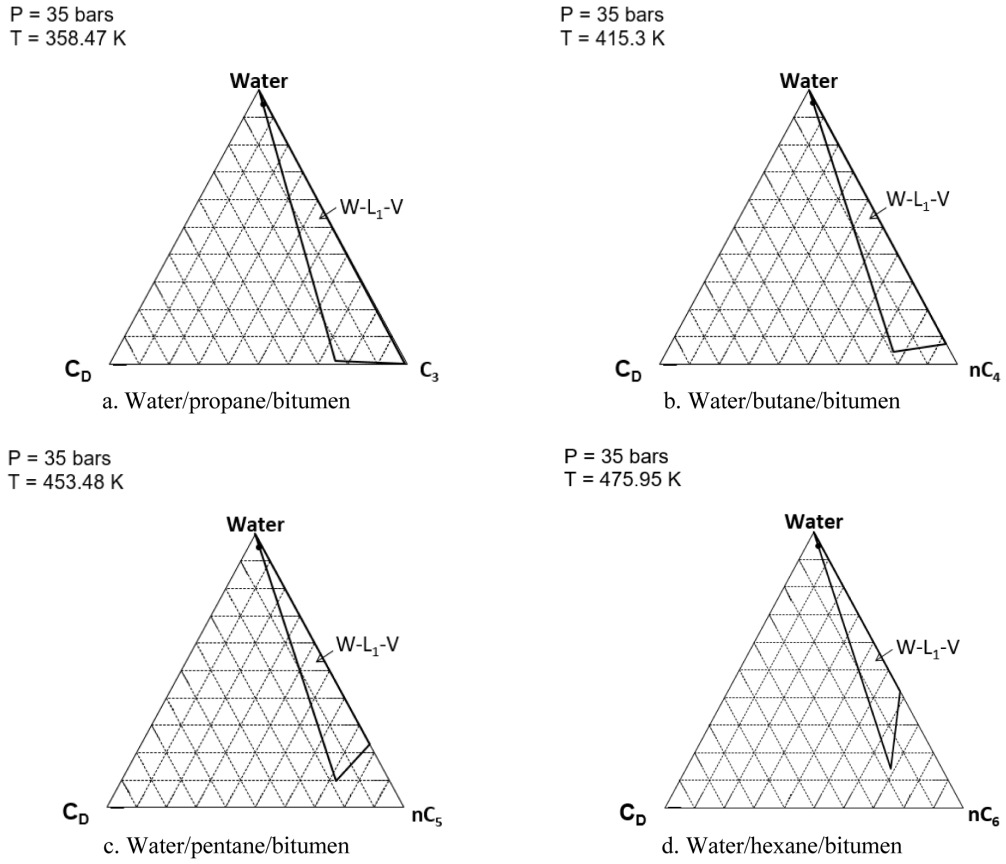

Figure 4—Vapor-condensation temperatures at 35 bars for water/solvent/bitumen mixtures for a fixed overall composition 95 mol% water, 4 mol% solvent, and 1 mol% bitumen (C_D). Four different alkane solvents are compared, propane, butane, pentane, and hexane. The overall composition is shown as the black dot located on the W-L edge of the tie triangle for the aqueous (W), oleic (L), and vapor (V) phases. The Peng-Robinson equation of state was used for the calculations (Tables 1 and 2). Two-phase regions associated with the tie triangle are omitted for clarity.

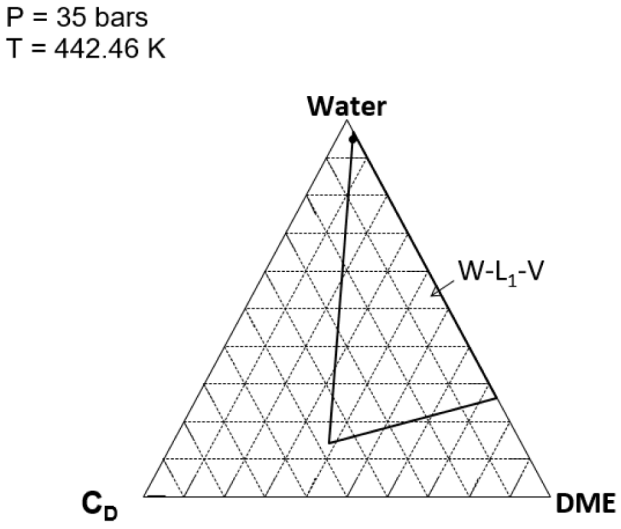

Figure 5—Vapor-condensation temperature at 35 bars for the overall composition 95 mol% water, 4 mol % DME, and 1 mol% bitumen (C_D). This overall composition is shown as the black dot located on the W-L edge of the tie triangle for the aqueous (W), oleic (L), and vapor (V) phases. The Peng-Robinson equation of state was used for the calculations. Two-phase regions associated with the tie triangle are omitted for clarity.

Figure 6 compares the temperature-composition (T-x) diagrams for water/C_5/C_D and water/DME/C_D at 35 bars. There are two separate three-phase regions for each diagram: W-L_1-V at higher temperature and W-L_1-

L_2 at lower temperature, where L_1 is the bitumen-rich liquid phase, and L_2 is the solvent-rich liquid phase. Two-phase regions associated with the three-phase regions are not shown for clarity. The ternary diagrams given in Figures 4 and 5 correspond to temperature cross-sections inside the W-L_1-V region in Figure 6. Figure 6 clearly shows that the lower-temperature limit for W-L_1-V is substantially lower in the water/DME/C_D system than in the water/C_5/C_D system. This is a direct consequence of the difference between the three-phase temperature for water/DME and that for water/C_5 at 35 bars, which are 382.18 K and 448.37 K, respectively, as shown in Figure 3. However, only one mol% of bitumen (C_D) in the overall composition makes the vapor-condensation temperature 60 K higher as discussed with Figure 5.

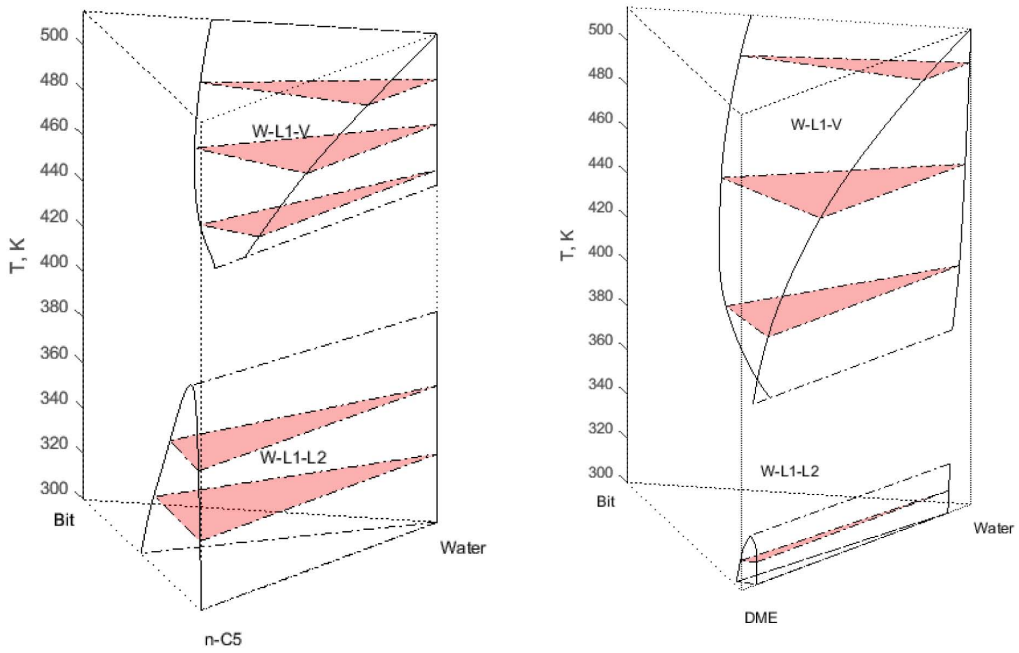

a. Water/pentane/bitumen b. Water/DME/bitumen

Figure 6—Temperature-composition diagramsfor water/solvent/bitumen at 35 bars by use of the PR-EOS model (Tables 1 and 2). Only three-phase regions are shown for clarity.

Figure 6 shows liquid-liquid separation of bitumen/solvent mixtures in the presence of the W phase in the W-L_1-L_2 region. Such phase behavior was experimentally observed in Gao et al. (2016) for water/C_4/Athabasca-bitumen mixtures. Based on the experimental observation, they stated that the liquid-liquid separation would limit the solubility of solvent in bitumen even when a high level of solvent accumulation took place near the edge of a steam chamber in solvent-SAGD with highly volatile solvents. Figure 6 shows that the upper-temperature limit for W-L_1-L_2 is calculated to be lower for the DME case than for the C_5 case. This indicates that the detrimental effect of W-L_1-L_2 phase behavior on bitumen dilution is less likely for DME-SAGD than forsolvent-SAGD with solvents that are less volatile than DME, such as C_5; however, further investigation into bitumen dilution by DME is necessary with more experimental data.

3. Simulation case study

This section presents a simulation case study to compare SAGD, DME-SAGD, and C_4-SAGD. The comparison between SAGD and DME-SAGD is to see the effect of solvent on SAGD in terms of bitumen-production rate, CSOR, and ultimate oil recovery. The comparison between DME-SAGD and C_4-SAGD is to see the effect of the solubility of solvent in water on the above-mentioned metrics and solvent recovery. DME and C_4 are compared because of the similarity in terms of volatility (Figure 3). Although the volatility of DME is closer to that of C_3 than C_4 (Figure 3), C_3 is not selected in this case study because it does not

improve SAGD for the bitumen reservoir considered here. Section 3.1 describes the simulation conditions. Results are discussed in Section 3.2.

3.1 Simulation model

With the CMG STARS simulator (Computer Modelling Group 2014), one half of a steam chamber is simulated for a homogeneous reservoir of 70 m (x) × 37.5 m (y) × 20 m (z). The reservoir is discretized into 70 × 1 × 20 gridblocks; that is, this is a vertical 2-D model. The temperature and pressure of the initial reservoir are 15 bars and 286.15 K, respectively. The reservoir initially contains 25% water and 75% live bitumen with a gas-oil ratio (GOR) of 0.44 m^3/m^3. The production well is placed at 3 m above the reservoir bottom, and the injection well is placed 4 m above the production well. The injection and production wells are operated at 35 bars and 15 bars, respectively. Other reservoir and well-pair parameters are summarized in Table 3.

Table 3—Input parameters for the simulation case study for SAGD and solvent-SAGD with the STARS simulator [Computer Modelling Group (CMG), 2014].

Porosity	33%
Horizontal permeability	4000 md
Vertical permeability	3000 md
Initial reservoir pressure at the depth of 500 m	15 bars
Initial reservoir temperature	286.15 K
Initial oil saturation	0.75
Initial water saturation	0.25
Three-phase relative permeability model (CMG 2014)	Stone's model II
Formation compressibility	1.8×10^{-3}1/bar
Rock heat capacity (Keshavarz et al. 2014)	2600 kJ/(m^3 K)
Rock thermal conductivity (Keshavarz et al. 2014)	660 kJ/(m day K)
Over/underburden heat capacity (Keshavarz et al. 2014)	2600 kJ/(m^3 K)
Over/underburden thermal conductivity (Keshavarz et al. 2014)	660 kJ/(m day K)
Bitumen thermal conductivity	11.5 kJ/(m day K)
Gas thermal conductivity	2.89 kJ/(m day K)
Producer bottom-hole pressure (minimum)	15 bars
Steam quality	0.9

All simulations are conducted for 10 years of operation. The reservoir is first preheated for 6 months. Then, 2 mol% of solvent is coinjected with steam at 35 bars until the steam chamber reaches the side boundary of the reservoir model. After the coinjection period, 100%wet steam of 90% quality is injected until the end of the operation. This is because bitumen recovery gradually becomes less efficient, and solvent recovery becomes the focus in the final stage.

The viscosity model for water/n-alkane/bitumen isthe same as those used in Venkatramani and Okuno (2016). That is, it takes into account the effect of water solubility in oil on L-phase viscosity. It also represents the difference between the mixing of water/bitumen and that of solvent/bitumen in terms of L-phase viscosity. Details of viscosities for water, n-alkanes, and bitumen as well as mixing coefficients for bitumen and n-alkanes can be found in their paper.

The correlation for viscosity of saturated-liquid DME by Wu et al. (2003) has been used to create a viscosity-temperature table at DME's subcritical conditions for STARS. The correlation is as follows:

$$\log_{10}\mu = -5.7282 + \frac{631.031}{T} + 0.01453T - 1.8225\times10^{-5}T^2, \quad (3)$$

where μ is DME viscosity in cp, and T is temperature in K. This correlation gives 0.5% AARD from experimental data measured from 227 K to 343 K. DME is supercritical above 400.05 K (Table 1). To our knowledge, however, no data is available for viscosity of supercritical DME. Therefore, it is assumed to be the same as the supercritical viscosity of C_3 in this research. Coefficients in the viscosity mixing rule for C_4 are used for DME in the absence of experimental viscosity data for bitumen/DME mixtures.

The STARS simulator models the V-phase densities by the ideal-gas law. The liquid phases' densities can be calculated by the following mixing rule (no volume change on mixing):

$$1/\rho_j = \sum_{i=1}^{Nc} x_{ij}/\rho_{ij}, \quad (4)$$

where ρ_j the molar density of liquid phase j, $x_{ij}$the mole fraction of component i in liquid phase j, and N_C is the number of components. ρ_{ij} is the molar density of component i in phase j at T and P, which can be calculated as follows:

$$\rho_{ij} = \rho_{iref}\exp[-\alpha_1(T-T_{ref}) - \frac{1}{2}\alpha_2(T^2 - T_{ref}^2) + \alpha_3(P-P_{ref}) + \alpha_4(P-P_{ref})(T-T_{ref})], \quad (5)$$

where P_{ref} is the reference pressure in kPa, 101.325 kPa, and T_{ref} isthe reference temperature in K, 288.15 K. ρ_{iref}isthe molar density of component i at the reference pressure and temperature. α's are coefficients, and can be obtained together with ρ_{iref} by regression to experimental data.

Densities for water, bitumen, and n-alkanes in this paper were taken by Venkatramani and Okuno (2016). Modified Rackett equations (Rackett 1970; Spencer and Danner 1972) were used by Ihmels and Lemmon (2007) for accurate representation of liquid DME density from 10 bars to 400 bars and 273 K to 523 K. The liquid density prediction from this model gives 0.039% AARD from experimental data. The modified Rackett equationis

$$\rho = \frac{\rho_0}{[1-C_T\ln((B_T+P)/(B_T+P_0))]}, \quad (6)$$

where $\rho_0 = \frac{A_R}{B_R^{[1+(1-\frac{T}{C_R})^{D_R}]}}$ and $B_T = B_{T0} + B_{T1}\frac{T}{E_T} + B_{T2}(\frac{T}{E_T})^2$. ρ is the liquid molar density of DME in mol/m³. T and P are temperature and pressure in K and MPa, respectively. C_T = 0.0834042, B_{T0} =284.304 MPa, B_{T1} = −130.021 MPa, B_{T2} = 14.4194 MPa, E_T = 100 K, A_R = 55.6001 mol/m³, B_R = 0.236704, C_R = 401.406 K, and D_R = 0.243368. The CMG STARS simulator uses the liquid density models described in equations 4 and 5, instead of the Rackett equation. Therefore, equations 4 and 5 were regressed to match predictions by the Rackett model up to 50 bars by adjusting the five parameters, ρ_{iref} and αh's. The regression results giveAAD and AARD of 14.9 kg/m³ and 2.7%, respectively, and are given in Tables 4 and 5 along with those coefficients for water, alkanes, and bitumen.

Table 4—Density coefficients for the simulation case study with the STARS simulator (Computer Modelling Group, 2014). Values for water and n-alkanes were taken from Venkatramani and Okuno (2016). The α values provided are for the use of equation 5 with the units of kPa and °C as required by STARS.

Component	ρ_{ref}, mol/m³	α_1, K⁻¹	α_2, K⁻²	α_3, kPa⁻¹	α_4, kPa⁻¹K⁻¹
Water	55425.9	-1.67×10^{-3}	6.48×10^{-6}	0.00	0.00
C_1	19959.5	1.32×10^{-3}	5.77×10^{-6}	5.13×10^{-6}	4.05×10^{-8}
n-C_4	13244.3	5.19×10^{-5}	5.05×10^{-6}	2.55×10^{-6}	4.56×10^{-9}
DME	15682.7	2.95×10^{-4}	9.98×10^{-6}	4.02×10^{-6}	6.14×10^{-7}

Table 5—Bitumen density coefficients for CMG STARS (2014) in the simulation case studies (Venkatramani and Okuno, 2016). The α values provided are for the use of equation 5 with the units of kPa and °C as required by STARS.

System	ρ_{ref}, mol/m³	α_1, K^{-1}	α_2, K^{-2}	α_3, kPa^{-1}	α_4, kPa^{-1}K^{-1}
Water/n-C_4/C_D	1872.9	-2.23×10^{-5}	9.09×10^{-7}	3.88×10^{-7}	4.28×10^{-9}
Water/DME/C_D	1872.9	-1.95×10^{-5}	8.95×10^{-7}	3.85×10^{-7}	4.72×10^{-9}

The EOS models introduced in section 2 is used to generate K-value tables for phase equilibrium calculation in the STARS simulator (CMG 2014). In the tabulation of K-value tables, a possible solvent-rich liquid phase has been disregarded as required by the format of STARS' K-value tables. That is, the detrimental effect of liquid-liquid separation on bitumen dilution that can occur for C_4-SAGD is not simulated in this case study.

3.2 Simulation results

Figure 7 presents the cumulative bitumen production histories simulated for SAGD, DME-SAGD, and C_4-SAGD. The bitumen production rates of DME-SAGD is higher than SAGD. Besides, DME-SAGD yields 5% higher ultimate recovery of bitumen than SAGD owing to the distillation mechanism (Keshavarz et al. 2014). For the same reason, C_4-SAGD is able to achieve a similar ultimate recovery to DME-SAGD. C_4-SAGD alsoshowsthe highest rate of bitumen production among the three processes studied here. The steam chamber reaches the side boundary at 3.8 years in DME-SAGD, 2.7 years in SAGD, and 2.9 years in C_4-SAGD. Therefore, steam-solvent coinjection is terminated at 3.8 years in DME-SAGD and 2.9 years in C_4-SAGD

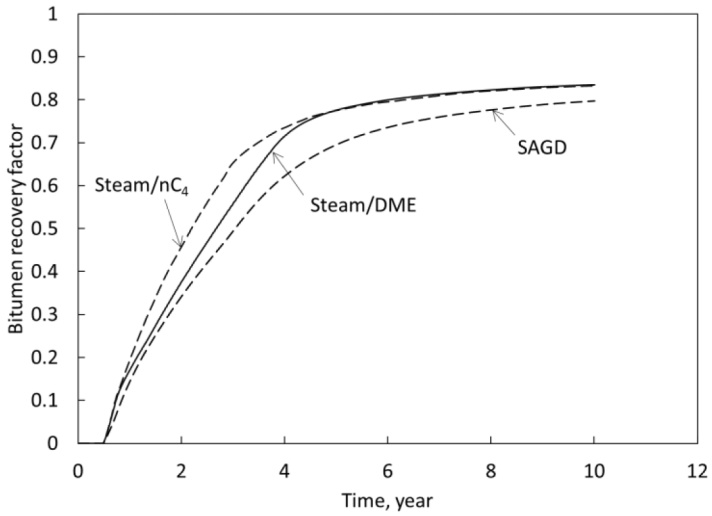

Figure 7—Bitumen recovery histories for steam-nC_4, steam-DME, and SAGD simulations.

Figure 8 shows the CSOR histories simulated for SAGD, DME-SAGD, and C_4-SAGD. DME-SAGD reduces CSOR by approximately 2 m³/m³ in comparison with SAGD, andC_4-SAGD reduces it even more in this case. The reduction in CSOR is owing to the lower chamber temperature in solvent-SAGD (Keshavarz et al. 2015).Figure 9 shows the temperature profiles near the steam-chamber edge for the 12th row from the reservoir top for SAGD, DME-SAGD, and C_4-SAGD at 1.8 years. The chamber-edge temperature is 502 K for SAGD, 404 K for DME-SAGD, and 381 K for C_4-SAGD in this figure. As expected from the analysis given in the previous section, the chamber-edge temperature in DME-SAGD is simulated to be 23 K higher than that in C_4-SAGD, in spite of the higher volatility of DMEin comparison with C_4 (Figure 3).

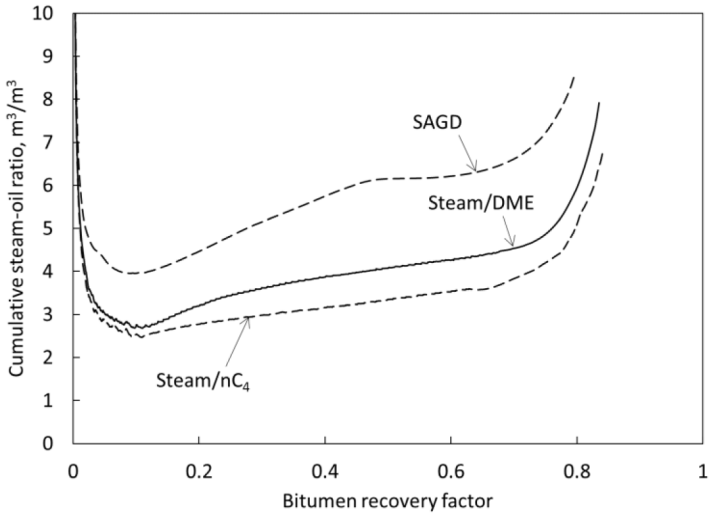

Figure 8—Cumulative steam-oil ratio for steam-nC_4, steam-DME, and SAGD simulations.

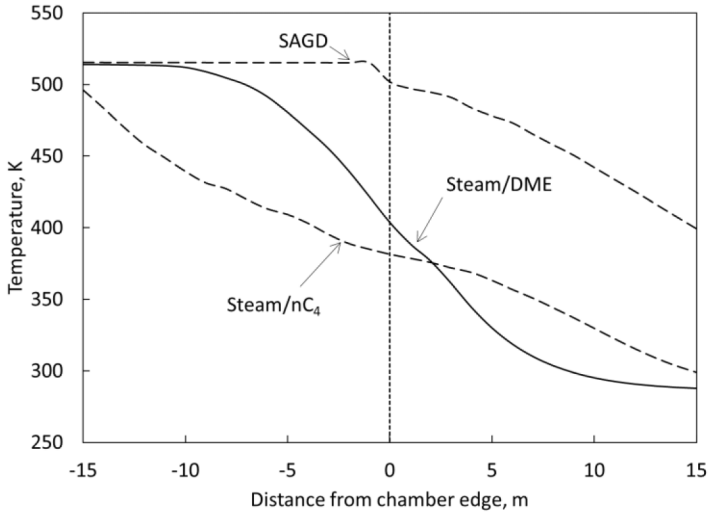

Figure 9—Temperature profiles near the steam-chamber edge for the 12th row form the reservoir top at 1.8 years forsteam-nC_4, steam-DME, and SAGD simulations. The dashed line indicates the edge of a steam chamber, the left side of which is the steam chamber.

Figure 10 shows the solvent mole fractions in the L and W phases for the 12th row from the reservoir top for DME-SAGD and C_4-SAGD. The DME concentration in the W phase is approximately 5 mol% within a few meters outside the chamber edge, which is consistent with Figure 5. The L phase near the chamber edge contains approximately 90 mol% C_4 in C_4-SAGD, and a smaller amount of DME in DME-SAGD, as shown in Figure 10a. This is qualitatively consistent with Figures 4 and 5, in which the L phase contains less than 40 mol% DME in Figure 5, but more than 75 mol% C_4 in Figure 4 (vapor-condensation conditions for a fixed overall composition at 35 bars). In DME-SAGD, the dilution of bitumen by DME shown in Figure 10a results in a SAGD-like bitumen production rate (Figure 7) while reducing SOR by 2 m^3/m^3 as shown in Figure 8.

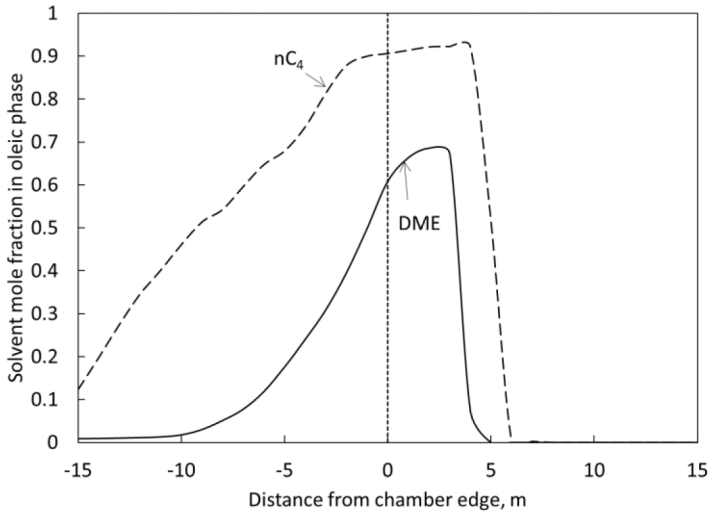

a. Solvent mole fraction in the L phase

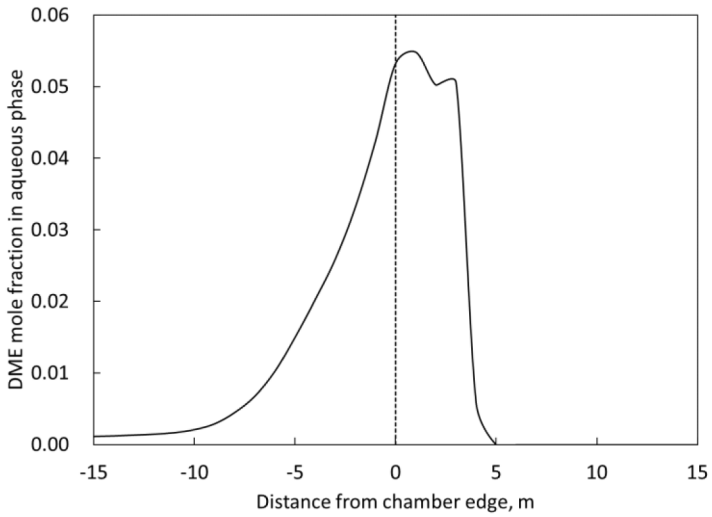

b. Solvent mole fraction in the W phase

Figure 10—Solvent mole fractions in the L and W phases for the 12th row from the reservoir top for DME-SAGD and C4-SAGD simulations; a. L phase, and b. W phase. The dashed line indicates the edge of a steam chamber, the left side of which is the steam chamber.

The solubility of DME in water results in the distribution of DME among phases in DME-SAGD that is substantially different from that of C_4in C_4-SAGD. Figure 11 presents the histories of solvent molar amounts in the V, L, and W phases for DME- and C_4-SAGD. In C_4-SAGD, a substantial amount of C_4 is present in the V phase, as is the case with solvent-SAGD by use of highly volatile solvents. At the moment the C_4 injection is terminated, approximately 50 mol% is in the L phase and 50 mol% is in the V phase. The solvent in the V phase decreases the in-situ temperature, which reduces heat losses to the overlying formation rocks and also facilitates the condensation of that solvent. However, the vapor solvent does not directly contribute to the dilution of bitumen. In DME-SAGD, the injected DME partitions into the W, L, and V phases inside the chamber and the W and L phases ahead of the chamber edge. Figure 11 shows that approximately 47 mol% of the in-situ DME is in the L phase, 41 mol% in the W phase, and 12 mol% in the V phase upon the termination of solvent injection. That is, a substantial amount of DME resides in the W phase; i.e., DME dilutes not only bitumen, but also water in DME-SAGD.

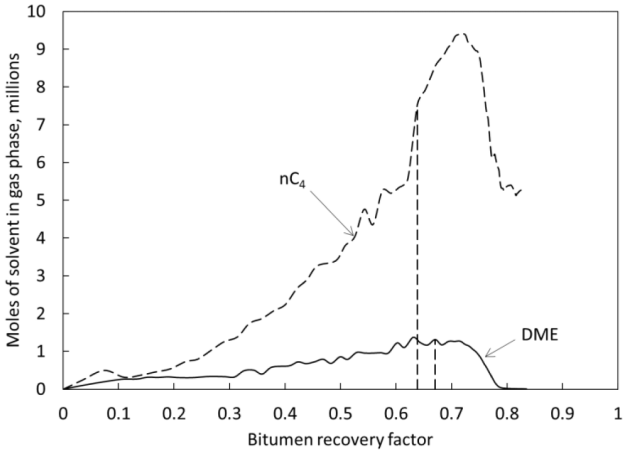

a. Solvent mole numbers in the V phase

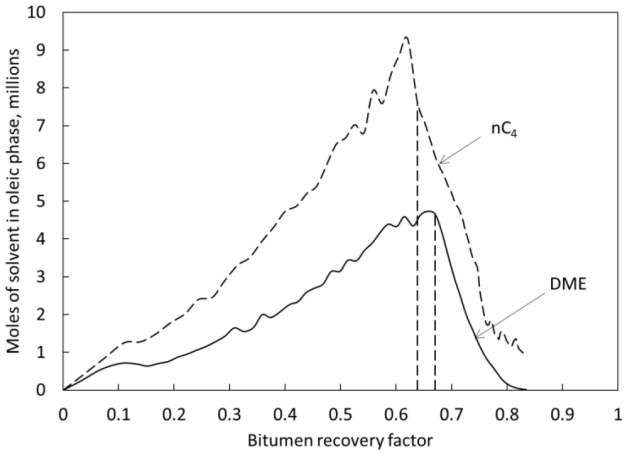

b. Solvent mole numbers in the L phase

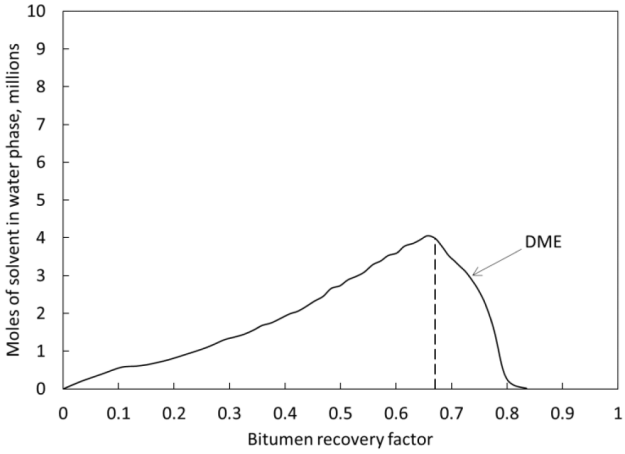

c. Solvent mole numbers in the W phase

Figure 11—Histories of solvent mole numbers in the V, L, and W phases for DME- and C_4-SAGD simulations. The dashed line indicates when the solvent injection is terminated.

Figure 12 shows the density distributions simulated for the W and L phases for DME-SAGD, C_4-SAGD, and SAGD for the 12th row from the reservoir top at 1.8 years. For DME-SAGD, the difference in mass density, $\Delta\rho_m$ (mass density of the W phase less mass density of the L phase), is nearly zero in the gravity-drainage zone outside the steam chamber and negative inside the steam chamber, because of the partitioning of DME into the W and L phases. However, $\Delta\rho_m$ is simulated to be systematically negative in SAGD and

positive in C_4-SAGD near the chamber edge. $\Delta\rho_m$ in the L-W two-phase flow along the chamber edge affects the compositional-flow regime, especially in solvent-SAGD.

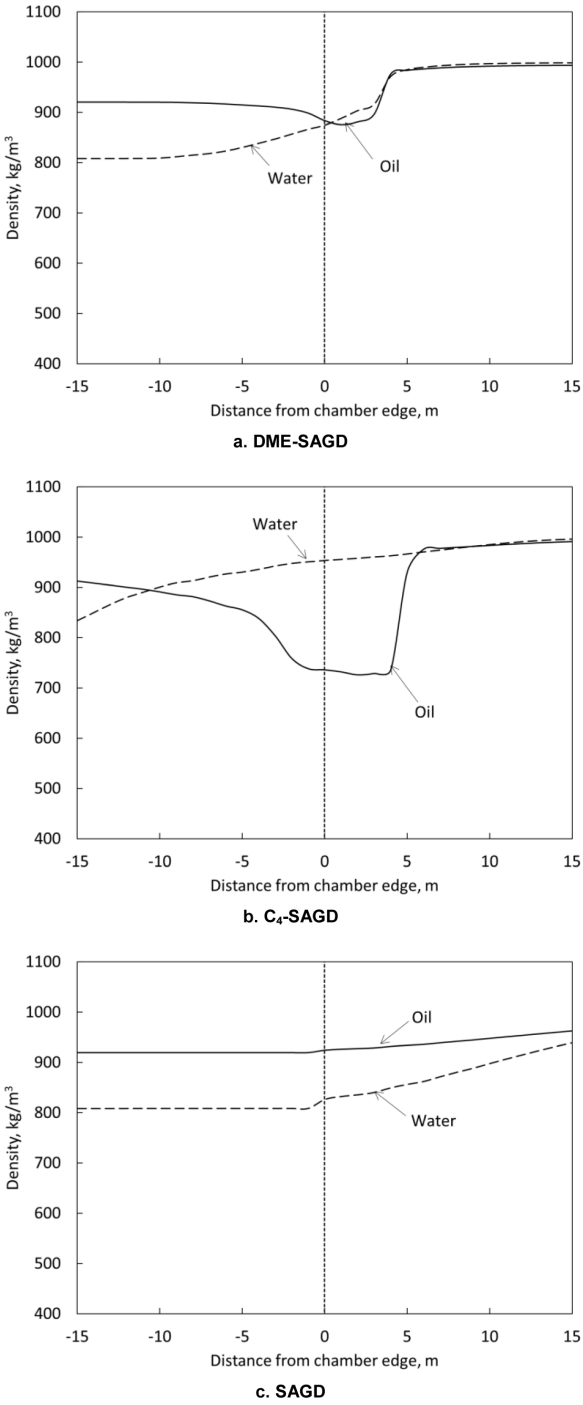

Figure 12—Density distributions simulated for the W and L phases for DME-SAGD, C_4-SAGD, and SAGD for the 12th row from the reservoir top at 1.8 years. The dashed line indicates the edge of a steam chamber, the left side of which is the steam chamber.

Figure 13 shows the molar flow rate of C_D in the L phase and that of water in the W phase in C_4-SAGD at 1.8 years. The chamber edge is indicated by black dots in this figure. The transport of bitumen (C_D) clearly occurs above that of water because the L phase is less dense than the W phase in C_4-SAGD as shown in Figure 12 for the 12th row. Figure 14 shows the molar flow rate of C_D in the L phase and that of water in the

W phase for DME-SAGD at 1.8 years. In DME-SAGD, the transport of C_D occurs more slowly, but in the thicker zone outside the chamber edge in comparison with C_4-SAGD (Figures 13a and 14a). DME appears to have penetrated deeper outside the chamber edge because of the lower level of gravity segregation between the L and W phases in DME-SAGD. This can be clearly seen in Figure 15, which shows the maps for the overall mole fraction of C_4 in C_4-SAGD and that of DME in DME-SAGD at 1.8 years. Figure 16 presents the profiles of overall composition for DME-SAGD, C_4-SAGD, and SAGD at the 12th row from the reservoir top at 1.8 years. The overall concentration of DME is higher outside the chamber than inside the chamber in DME-SAGD. This is in contrast to the C_4 concentration profile shown in Figure 16b for C_4-SAGD. In C_4-SAGD, a substantial amount of C_4 is used to transport a small amount of bitumen (C_D) (approximately 1 mol% in Figure 16a), which makes a C_4 bank flowing with the W phase with a large positive $\Delta\rho_m$. In DME-SAGD, a larger amount of C_D is diluted by a smaller amount of solvent, and the segregation of the L and W phases is less clear (Figure 16ac).

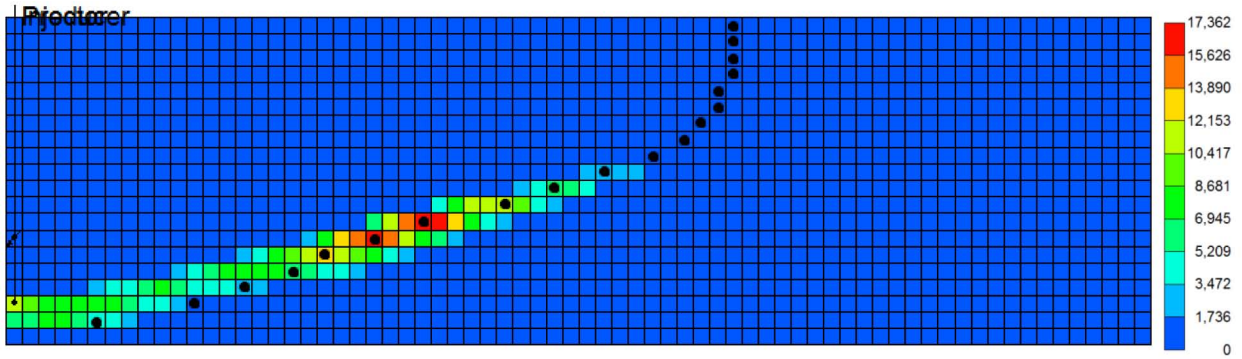

a. **Molar flow rate of C_D in the L phase**

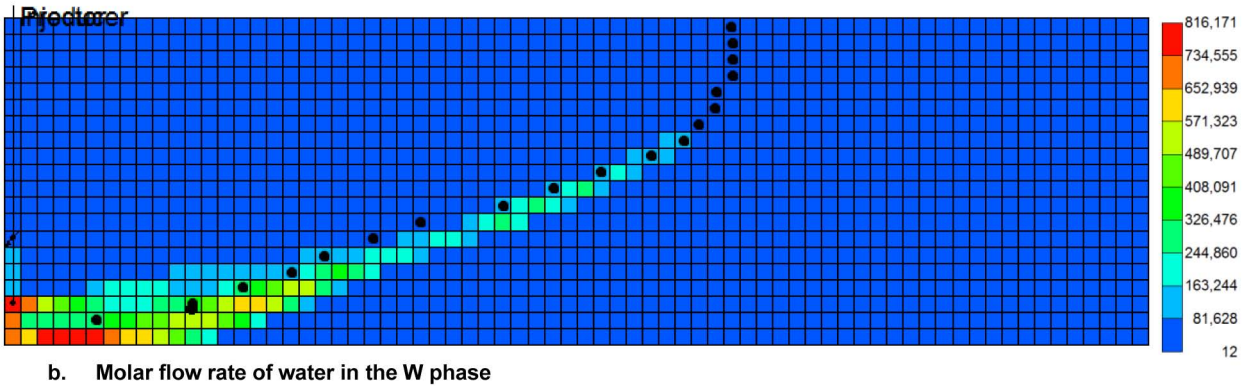

b. **Molar flow rate of water in the W phase**

Figure 13—2-D maps for (a) molar flow rate of the bitumen component (C_D) in the L phase (moles/day), and (b) molar flow rate of water in the W phase (moles/day) in C_4-SAGD at 1.8 years. The chamber edge is indicated by black dots.

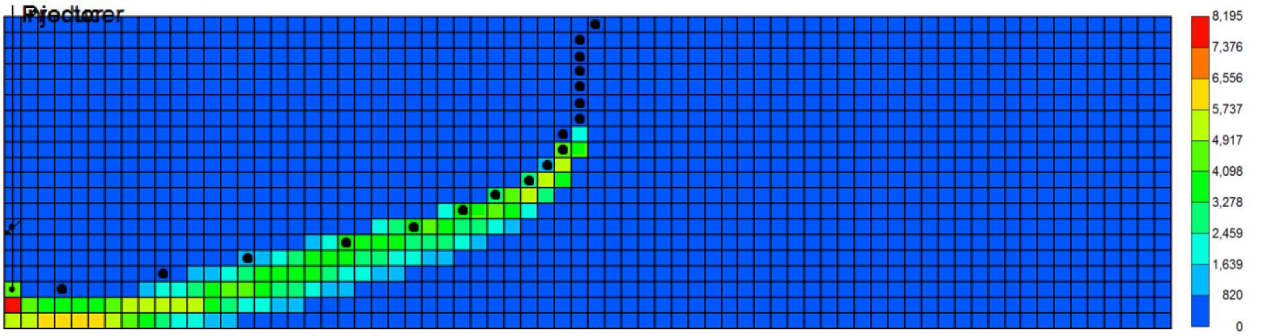

a. Molar flow rate of C_D in the L phase

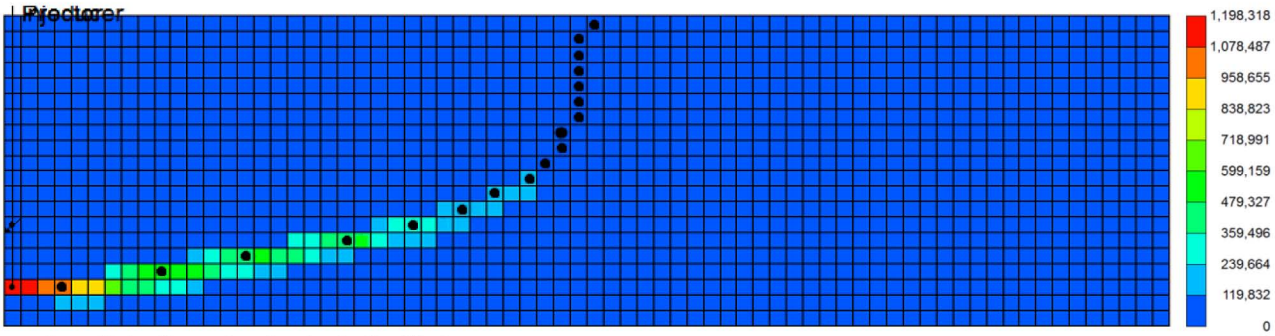

b. Molar flow rate of water in the W phase

Figure 14—2-D maps for (a) molar flow rate of the bitumen component (C_D) in the L phase (moles/day), and (b) molar flow rate of water in the W phase (moles/day) in DME-SAGD at 1.8 years. The chamber edge is indicated by black dots.

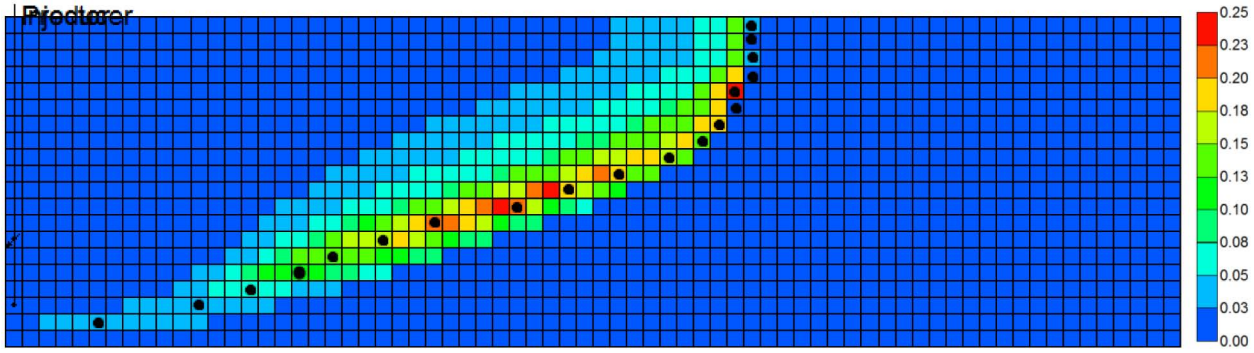

a. C_4 distribution in C_4-SAGD

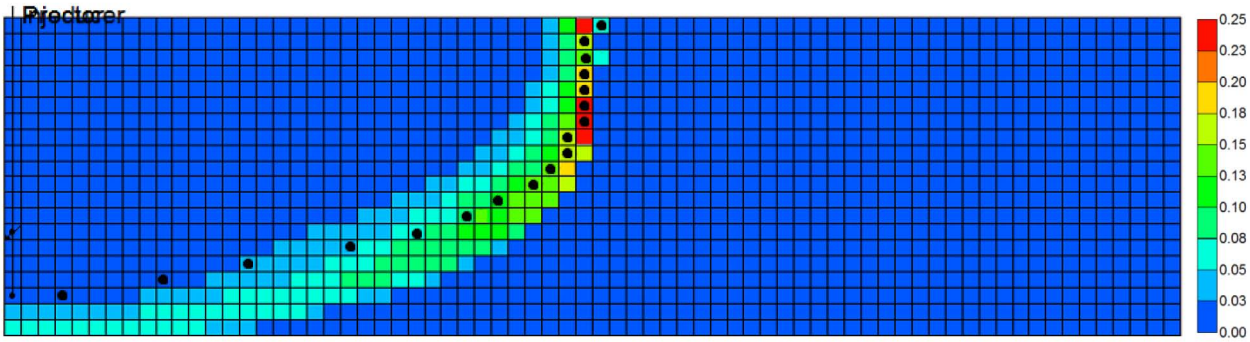

b. DME distribution in DME-SAGD

Figure 15—Overall concentration of C_4 in C_4-SAGD and that of DME in DME-SAGD at 1.8 years. The chamber edge is indicated by black dots.

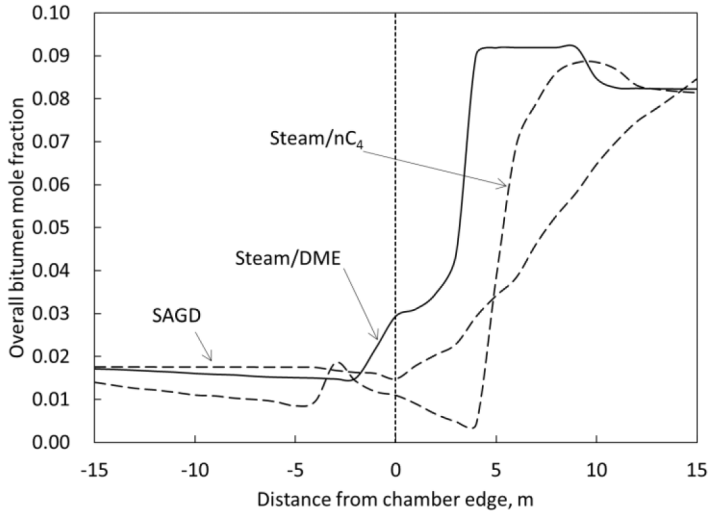

a. Bitumen component

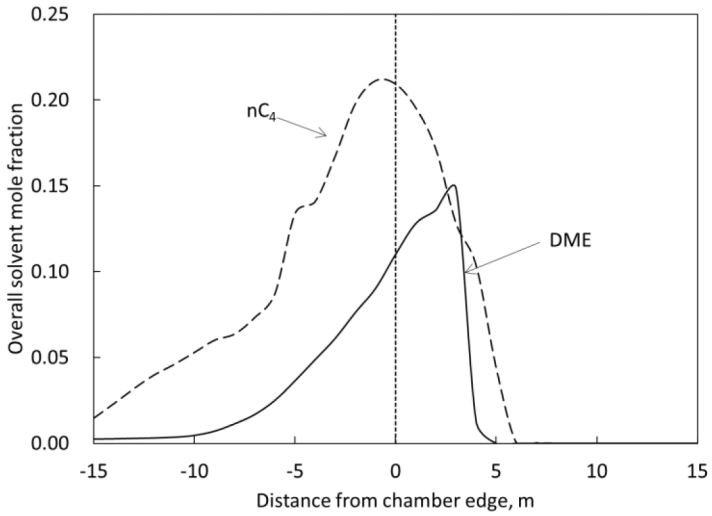

b. Solvent component

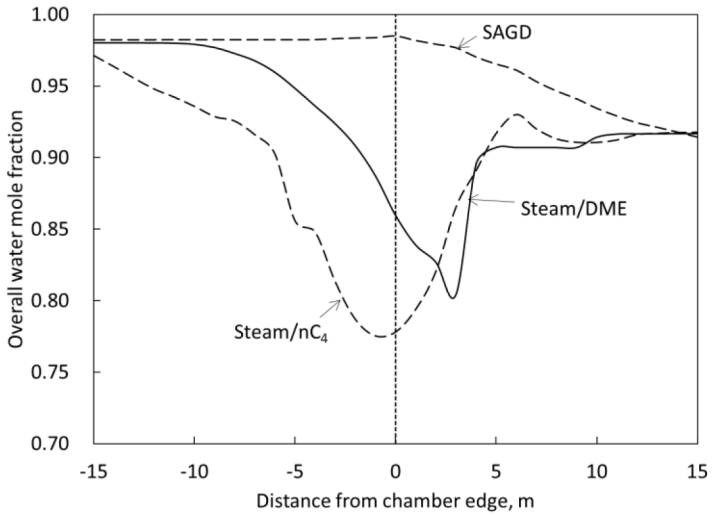

c. Water component

Figure 16—Profiles of overall composition for DME-SAGD, C_4-SAGD, and SAGD at the 12throw from the reservoir top at 1.8 years. The dashed line indicates the edge of a steam chamber, the left side of which is the steam chamber.

The DME distribution among phases given in Figure 11 also improves solvent recovery in DME-SAGD in comparison with C_4-SAGD. Figure 17 shows that the solvent recovery factor in DME-SAGD is systematically higher than that of C_4-SAGD (approximately by 15%). The solvent recovery factor is defined here as the cumulative volume of solvent produced divided by the cumulative volume of solvent injected at a given time. In DME-SAGD, 92% of DME is recovered by the produced W phase, and 10% from the produced L phase measured at the reservoir conditions. In C_4-SAGD, 100% of C_4 is from the produced L phases since C_4 is insoluble in water.

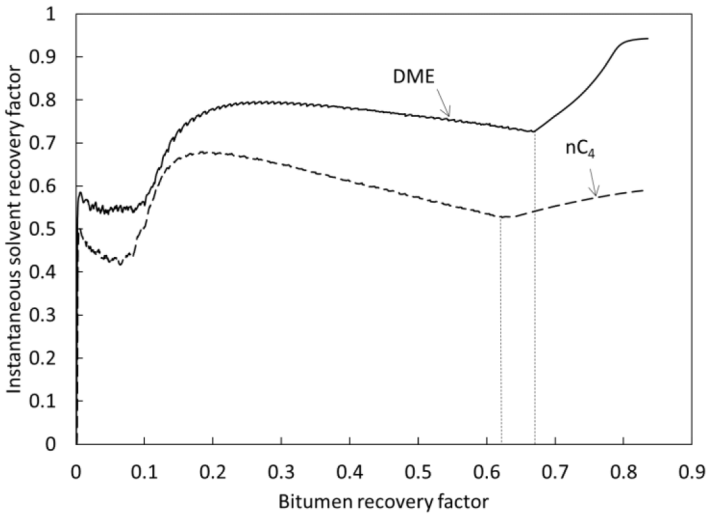

Figure 17—Solvent-recovery factor for DME-SAGD and C_4-SAGD. The recovery factor is defined here as the cumulative volume of solvent produced divided by the cumulative volume of solvent injected at a given time. The dashed line indicates when the solvent injection is terminated.

4. Conclusions

This paper was concerned with the potential of water-soluble solvent as an additive to steam for improving the efficiency of SAGD. The main objective of this paper was to investigate how the solubility of solvent in water affects solvent-SAGD. DME and Athabasca bitumen were considered respectively as the water-soluble solvent and bitumen in this study. However, it is beyond the scope of this research to single out a particular compound as a promising water-soluble additive to steam for a given bitumen/heavy oil. Conclusions are as follows:

- Although DME is more volatile than C_4, the solubility of DME in water in DME-SAGD results in chamber-edge temperatures that are higher than those in C_4-SAGD. This can be explained by ternary phase behavior of water/solvent/bitumen mixtures; that is, the transition from WLV to WL for such a system tends to occur at a higher temperature for a given overall composition and pressure when the solvent partitions into the W phase.
- The solubility of DME in bitumen is nearly a half of that of C_4 at their corresponding chamber-edge conditions (Figures 4, 5, and 10). In DME-SAGD simulations, however, approximately47 mol% of the in-situ DME was used for dilution of bitumen, which was equivalent to the fraction of the in-situ C_4 used for bitumen dilution in C_4-SAGD. This occurslikely because the partitioning of DME into bitumen and water reduces the gravity segregation of the two-liquid-phase flow along the edge of a steam chamber in DME-SAGD. The reduced gravity segregation in DME-SAGD is expected to facilitate the mixing of condensed DME with bitumen. This is in contrast to C_4-SAGD, in which the L phase diluted by a substantial amount of C_4 is much less dense than the W phase, impeding thecontact between the C_4bank and bitumen along the edge of a steam chamber.

- Simulation results showed that the vapor fraction of the in-situ solvent was much smaller in DME-SAGD than in C_4-SAGD. Also, the injected DME can be recovered not only by the L phase, but also by the W phase in DME-SAGD. Therefore, the recovery factor of solvent was simulated to be systematically higher (by approximately 15%) in DME-SAGD than in C_4-SAGD.
- Simulation results showed that DME-SAGD yielded 35% reduction in SOR in comparison with SAGD while being able to keep SAGD-like rates of bitumen production. DME-SAGD also resulted in 5% higher ultimate recovery of bitumen than SAGD. However, C_4-SAGD was simulated to be superior to DME-SAGD in terms of bitumen-production rate and SOR in the case studied.

Acknowledgements

We gratefully acknowledge the financial support from Japan Petroleum Exploration Co., Ltd. and Japan Canada Oil Sands Ltd. Okuno holds the Pioneer Corporation Faculty Fellowship in Petroleum Engineering at The University of Texas at Austin.

Nomenclature

Roman Symbols

A, B, C, D and E = coefficients in the Rackett equation
L = oleic phase
P = pressure
S = saturation
T = temperature, K
V = vapor phase
V = volume, m^3
W = aqueous phase
x = mole fraction

Greek Symbols

α = density coefficient
μ = viscosity, mPa·s
ρ = molar density, mole/m^3
ω = acentric factor

Subscripts

bit = bitumen
c = critical condition
C_D = dead bitumen
HC = hydrocarbon
L = oleic phase
ref = reference condition
sol = solvent
V = vapor phase
w = water

Abbreviations

AAD = average absolute deviation
AARD = average absolute relative deviation
API = American petroleum institute

BIP = binary interaction parameter
CSOR = cumulative steam-to-oil ratio
CPA = cubic-plus-association
DME = dimethyl ether
EOS = equation of state
ES-SAGD = expanding-solvent-SAGD
GOR = gas-oil ratio
HV = Huron-Vidal
LASER = liquid-addition-to-steam-for-enhanced-recovery
MW = molecular weight, g/mol
PR = Peng and Robinson
SAGD = steam-assisted gravity drainage
SAP = solvent-aided-process
SOR = steam-oil ratio
UCEP = upper critical end point
vdW = van der Waals

References

Alkindi, A., Al-Azri, N., Said, D., AlShuaili, K., te Riele, P. 2016. Persistence in EOR-Design of a Field Trial in a Carbonate Reservoir Using Solvent-based Water-Flood Process. Presented at the SPE EOR Conference at Oil and Gas West Asia, Muscat, Oman, 21-23 March.

Amani, M.J., Gray, M.R. and Shaw, J.M. 2013. Phase Behavior of Athabasca Bitumen+ Water Mixtures at High Temperature and Pressure. *The Journal of Supercritical Fluids* **77**:142–152.

Amani, M.J., Gray, M.R. and Shaw, J.M. 2013. Volume of mixing and solubility of water in Athabasca bitumen at high temperature and pressure. *Fluid Phase Equilibria*, **358**: 203–211.

American Petroleum Institute, 1983. *API Technical Data Book – Petroleum Refining*, 4th Edition, American Petroleum Institute, New York, USA.

Brunner, E. 1990. Fluid Mixtures at High Pressures IX. Phase Separation and Critical Phenomena in 23 (n-alkane+ water) Mixtures. *The Journal of Chemical Thermodynamics* **22**(4), 335–353.

Butler, R. M. 1997. *Thermal Recovery of Oil and Bitumen*. Calgary, Alberta, Canada: GravDrain Inc.

Chahardowli, M., Farajzadeh, R., Bruining, H. 2016. Experimental Investigation of Dimethyl Ether/Polymer Hybrid as an Enhanced Oil Recovery Method. Presented at the SPE EOR Conference at Oil and Gas West Asia, Muscat, Oman, 21-23 March.

Chapman, W. G., Gubbins, K. E., Joslin, C. G., Gray, C. G. 1986. Theory and Simulation of Associating Liquid Mixtures. *Fluid Phase Equilibria***29**: 337–46.

Chernetsky, A., Masalmeh, S., Eikmans, D., Boerrigter, P. M., Fadili, A., Parsons, C. A., Parker, A., Boersma, D. M., Cui, J., Dindoruk, B., te Riele, P. M., Alkindi, A., Azri, N. 2015. A Novel Enhanced Oil Recovery Technique: Experimental Results and Modelling Workflow of DME Enhanced Waterflood Technology. Presented at the Abu Dhabi International Petroleum Exhibition and Conference, Abu Dhabi, UAE, 9-12 Nov.

Computer Modelling Group, 2014. *STARS version 2014user's guide*. Computer Modelling Group, Calgary, Alberta, Canada.

Constantinou, L. and Gani. R. 1994. New Group Contribution Method for Estimating Properties of Pure Compounds. *AIChE Journal***40** (10): 1697–1710.

Constantinou, L., Gani, R., O'Connell, J. P. 1995. Estimation of the Acentric Factor and the Liquid Molar Volume at 298 K Using a New Group Contribution Method. *Fluid Phase Equilibria*, **103**(1), 11–22.

Folas, G. K., Kontogeorgis, G. M., Michelsen, M. L., Stenby, E. H. 2006. Application of the Cubic-Plus Association Equation of State to Mixtures with Polar Chemicals and High Pressures. *Industrial & Engineering Chemistry Research* **45**: 1516–1526.

Folas, G. K., Kontogeorgis, G. M., Michelsen, M. L., Stenby, E. H. 2006. Application of the Cubic-Plus Association (CPA) Equation of State to Complex Mixtures with Aromatic Hydrocarbons. *Industrial & Engineering Chemistry Research* **45**: 1527–1538.

Ganjdanesh, R., Rezaveisi, M., Pope, G. A., Sepehrnoori, K. 2016. Treatment of Condensate and Water Blocks in Hydraulic-Fractured Shale-Gas Condensate Reservoirs. *SPE Journal*.

Gao, J., Okuno, R. and Li, H.A. 2016. An Experimental Study of Multiphase Behavior for n-Butane/Bitumen/Water Mixtures. *SPE Journal*. Accepted for publication. SPE-180736-PA

Gates, I. D., 2007. Oil Phase Viscosity Behavior in Expanding-Solvent Steam-Assisted Gravity Drainage. *Journal of Petroleum Science and Engineering***59** (1-2): 123–134.

Groot, J. A. W. M., Eikmans, D., Fadili, A., Romate, J. E. 2016. Field-Scale Modeling and Sensitivity Analysis of DME Enhanced Waterflooding. Presented at SPE EOR Conference at Oil and Gas West Asia, Muscat, Oman, 21-23, March.

Groot, J. A. W. M., Chernetsky, A., te Riele, P. M., Dindoruk, B., Cui, J., Wilson, L. C., Ratnakar, R. 2016. Representation of Phase Behavior and PVT Workflow for DME Enhanced Water-Flooding. Presented at the SPE EOR Conference at Oil and Gas West Asia, Muscat, Oman, 21-23, March.

Gupta, S., Gittins, S., Picherack, P. 2005. Field Implementation of Solvent Aided Process. *Journal of Canadian Petroleum Technology***44** (11): 8–13.

Gupta, S. C., Gittins, S. D. 2006. Christina Lake Solvent Aided Process Pilot. *Journal of Canadian Petroleum Technology***45** (9): 15–18.

Holldorff, H. and Knapp, H. 1988. Binary Vapor-Liquid-Liquid Equilibrium of Dimethyl Ether – Water and Mutual Solubilities of Methyl Chloride and Water. *Fluid Phase Equilibria***44**: 195–209.

Huron, M. J. and Vidal, J. 1979. New Mixing Rules in Simple Equations of State for Representing Vapour-Liquid Equilibria of Strongly Non-ideal Mixtures, *Fluid Phase Equilibria* **3**: 255–271

Ihmels, E. C., Lemmon, E. W. 2007. Experimental Densities, Vapor Pressures, and Critical Point, and a Fundamental Equation of State for Dimethyl Ether. *Fluid Phase Equilibria***260**: 36–48.

Ivory. J. J., Zheng, R., Nasr, T. N., Deng, X., Beaulieu, G., Heck, G. 2008. Investigation of Low Pressure ES-SAGD. Presented at 2008 SPE International Thermal Operations and Heavy Oil Symposium, Calgary, Alberta, Canada, October 20–23.

Keshavarz, M., Okuno, R., and Babadagli, T. 2014. Efficient Oil Displacement Near the Chamber Edge in ES-SAGD. *Journal of Petroleum Science and Engineering***118**: 99–113.

Keshavarz, M., Okuno, R., and Babadagli, T. 2015. Optimal Application Conditions for Steam/Solvent Coinjection. *SPE Reservoir Evaluation & Engineering***18** (1):20–38. SPE-165471-PA

Kontogeorgis, G. M., Voutsas, E. C., Yakoumis, I. V., Tassios, D. P. 1996. An Equation of State for Associating Fluids. *Industrial & Engineering Chemistry Research* **35**: 4310–4318.

Kumar, A. 2016. Characterization of Reservoir Fluids based on Perturbation from n-Alkanes. PhD dissertation, University of Alberta.

Kumar, A. and Okuno, R. 2016. Reliable Characterization of Bitumen Based on Perturbation from n-alkanes for Steam-solvent Coinjection Simulation. *Fuel* **182**: 141–153.

Leaute, R. P., 2002. Liquid Addition to Steam for Enhancing Recovery of Bitumen with CSS: Evolution of Technology from Research Concept to a Field Pilot at Cold Lake. SPE/Petroleum Society of CIM/CHOA Paper Number 79011, Calgary, Alberta, Canada, November 4–7.

Leaute, R. P., Carey, B. S. 2007. Liquid Addition to Steam for Enhancing Recovery (LASER) of Bitumen with CSS: Results from the First Pilot Cycle. *Journal of Canadian Petroleum Technology***46** (9).

Li. W., Mamora, D. D., Li, Y., 2011a. Light-and Heavy-Solvent Impacts on Solvent-Aided-SAGD Process: A Low – Pressure Experimental Study. *Journal of Canadian Petroleum Technology***50** (4): 19–30.

Li. W., Mamora, D. D., Li, Y., 2011b. Solvent-type and -ratio Impacts on Solvent-aided SAGD Process. *SPE Reservoir Evaluation & Engineering***14** (3):320–331.

Michelsen, M. L. A Modified Huron-Vidal Mixing Rule for Cubic Equations of State. *Fluid Phase Equilibria* **60**: 213–219.

Mohebati, M. H., Maini, B. B., and Harding, T. G. 2012. Numerical-Simulation Investigation of the Effect of Heavy-oil Viscosity on the Performance of Hydrocarbon Additives in SAGD. *SPE Reservoir Evaluation & Engineering***15** (02): 165–181.

Nasr, T. N., Beaulieu, G., Golbeck, H., Heck, G. 2003. Novel expanding solvent-SAGD process "ES-SAGD". *Journal of Canadian Petroleum Technology***42** (1): 13–16.

Oliveira, M. B., Coutinho, J. A. P., Queimada, A. J. 2007. Mutual Solubilities of Hydrocarbons and Water with the CPA EoS, *Fluid Phase Equilibria***258**: 58–66.

Park, K.J., Seo, T. and Jung, D. 2007. Performance of Alternative Refrigerants for Residential Air-Conditioning Applications. *Applied energy***84**: 985–991.

Parsons, C. Chernetsky, A. Eikmans, D., te Riele, P. Boersma, D., Sersic, I., Broos, R. 2016. Introducing a Novel Enhanced Oil Recovery Technology. Presented at the SPE Improved Oil Recovery Conference, Tulsa, Oklahoma, USA, April 11–13.

Pedersen, K. S., Christensen, P. L., Shaikh, J. A. 2014. *Phase Behavior of Petroleum Reservoir Fluids*, CRC Press.

Pozo, M. E. and Streett, W. B. 1984. Fluid Phase Equilibria for the System Dimethyl Ether/Water from 50 to 220 C and Pressures to 50.9 MPa. *Journal of Chemical & Engineering Data* **29**: 324–329.

Rackett, H.G. 1970. Equation of State for Saturated Liquids. *Journal of Chemical and Engineering Data* **15**(4):514–517.

Ratnakar, R. R., Dindoruk, B., Wilson, L. 2016a. Experimental Investigation of DME-Water-Crude Oil Phase Behavior and PVT Modeling for the Application of DME-Enhanced Waterflooding. *Fuel***182** (2016): 188–197.

Ratnakar, R. R., Dindoruk, B., Wilson, L. 2016b. Phase Behavior Experiments and PVT Modeling of DME-Brine-Crude Oil Mixtures Based on Huron-Vidal Mixing Rules for EOR Applications. *Fluid Phase Equilibria*.

Riazi, M.R. and Daubert, T.E. 1987. Characterization Parameters for Petroleum Fractions. *Industrial & engineering chemistry research*, **26**: 755–759.

Robinson, D. B., Peng, D. Y. 1978. Gas Processors Association. *Research Report RR-28*

Scharlin, P., Battino, R., Silla, E., Tunon, I. and Pascual-Ahuir, J.L. 1998. Solubility of Gases in Water: Correlation Between Solubility and the Number of Water Molecules in the First Solvation Shell. *Pure and applied chemistry*, **70**:1895–1904.

Shen, C. 2013. *Enhanced Oil Recovery Field Case studies*. 1st Edition. Chapter 13, pp. 413 – 455, Elsevier.

Soave G. 1972. Equilibrium Constants from a Modified Redlich-Kwong Equation of State. *Chemical Engineering Science***27**: 1197–1203.

Spencer, C.F. and Danner, R.P. 1972. Improved Equation for Prediction of Saturated Liquid Density. *Journal of Chemical and Engineering Data* **17**(2):236–241.

Tallon, S. and Fenton, K. 2010. The Solubility of Water in Mixtures of Dimethyl Ether and Carbon Dioxide. *Fluid Phase Equilibria*, **298**: 60–66.

Te Riele, P., Parsons, C., Boerrigter, P., Plantenberg, J., Suijkerbuijk, B., Burggraaf, J., Chernetsky, A., Boersma, D., Broos. R. 2016. Implementing a Water Soluble Solvent Based Enhanced Oil Recovery Technology-Aspects of Field Development Planning. Presented at the SPE EOR Conference at Oil and Gas West Asia, Muscat, Oman, 21-23, March.

Venkatramani, A. and Okuno, R. 2015. Characterization of Water-Containing Reservoir Oil Using an EOS for Steam Injection Processes. *Journal of Natural Gas Science and Engineering* **26**:1091–1106.

Venkatramani, A., Okuno, R. 2016. Compositional Mechanisms in SAGD and ES-SAGD With Consideration of Water Solubility in Oil. *SPE Reservoir Evaluation & Engineering*. SPE-180737-PA

Venkatramani, A. and Okuno, R. 2017. Steam-Solvent Coinjection under Reservoir Heterogeneity: Should ES-SAGD be Implemented for Highly Heterogeneous Reservoirs? Presented at the SPE Canada Heavy Oil Conference, Calgary, Alberta, Canada. 15 – 16 February. SPE-185001-MS

Wu, J., Liu, Z., Bi, S., Meng, X. 2003. Viscosity of Saturated Liquid Dimethyl Ether from (227 to 343) K. *Journal of Chemical & Engineering Data* **48**: 426–429.

Wu. J., Liu, Z., Wang, B., Pan, J. 2004. Measurement of the Critical Parameters and the Saturation Densities of Dimethyl Ether. *Journal of Chemical & Engineering Data* **49**: 704–708.

Wu, J. and Yin, J. 2008. Vapor Pressure Measurements of Dimethyl Ether From (213 to 393) K. *Journal of Chemical & Engineering Data* **53**: 2247–2249.

Zhu, D. and Okuno, R. 2016. Multiphase Isenthalpic Flash Integrated with Stability Analysis. *Fluid Phase Equilibria***423**: 203–219